Supplement of Atmos. Chem. Phys., 19, 4561–4594, 2019
https://doi.org/10.5194/acp-19-4561-2019-supplement

Atmospheric Chemistry and Physics
Open Access
EGU

Supplement of

Simulating secondary organic aerosol in a regional air quality model using the statistical oxidation model – Part 3: Assessing the influence of semi-volatile and intermediate-volatility organic compounds and NO_x

Ali Akherati et al.

Correspondence to: Shantanu H. Jathar (shantanu.jathar@colostate.edu)

Simulating secondary organic aerosol in a regional air quality model using the statistical oxidation model – Part 3: Assessing the influence of semi-volatile and intermediate volatility organic compounds and NO_x

Ali Akherati[1], Christopher D. Cappa[2], Michael J. Kleeman[2], Kenneth S. Docherty[3], Jose L. Jimenez[4], Stephen M. Griffith[5], Sebastien Dusanter[6], Philip S. Stevens[5], and Shantanu H. Jathar[1]

[1]Department of Mechanical Engineering, Colorado State University, Fort Collins, CO, USA
[2]Department of Civil and Environmental Engineering, University of California Davis, Davis, CA, USA
[3]Jacobs Technology, Raleigh, NC, USA
[4]Department of Chemistry and Cooperative Institute for Research in Environmental Sciences (CIRES), University of Colorado, Boulder, CO, USA
[5]School of Public and Environmental Affairs and Department of Chemistry, Indiana University, Bloomington, IN, USA
[6]IMT Lille Douai, Univ. Lille, SAGE - Département Sciences de l'Atmosphère et Génie de l'Environnement, 59000 Lille, France
Correspondence to: Shantanu H. Jathar (shantanu.jathar@colostate.edu)

Figures

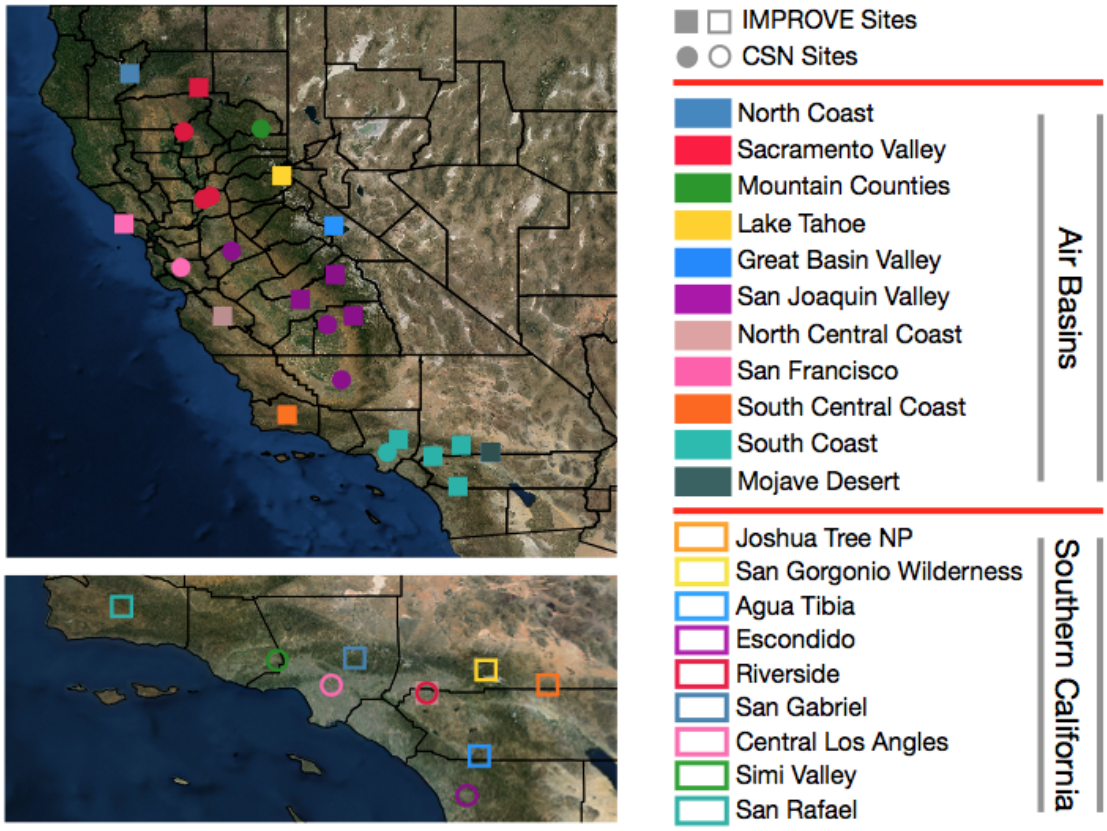

Figure S1: Model domains showing the 24 km grid (top) used for the state of California simulations and the 8 km nested grid (bottom) used for the southern California simulations. Symbols show the Chemical Speciation Network (CSN) and Interagency Monitoring of Protected Visual Environments (IMPROVE) network sites in both domains.

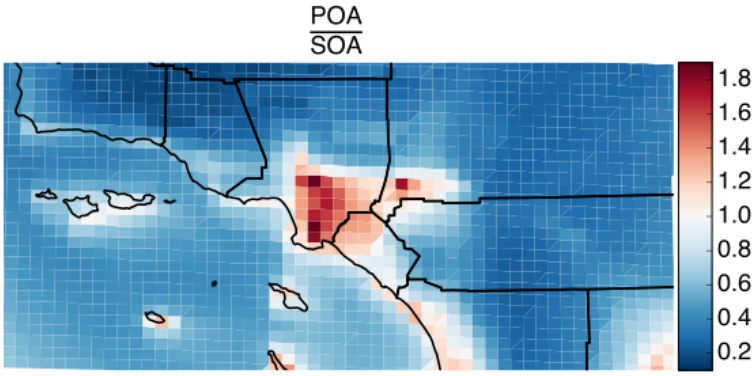

Figure S2: Ratio of the 14-day averaged POA mass concentration to SOA_{eff} mass concentration in the Base simulation.

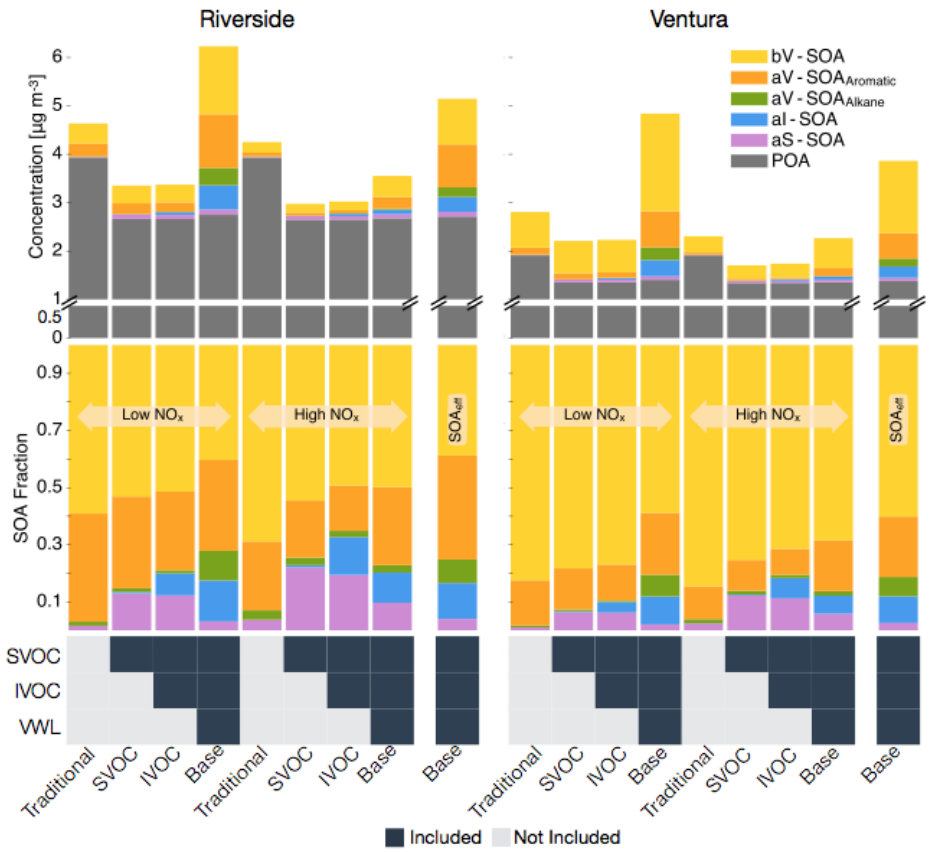

Figure S3: 14-day averaged model predictions of POA and SOA mass concentrations and precursor contributions at the (a) Riverside and (b) Simi Valley site from the sensitivity simulations that examine the influence of updates made in this work. Panel (a) shows absolute concentrations and panel (b) shows precursor contributions. The legend at the bottom tracks how the different pathways (i.e., SOA formation from SVOCs, SOA formation from IVOCs, and correction for chamber vapor wall losses (VWL)) were turned on for the different simulations. Model predictions from the low and high NO_X simulations are shown separately. Model predictions to the extreme right are from accounting for the influence of NO_X using equation 2 in the main text (logarithmic dependence on VOC:NO_X).

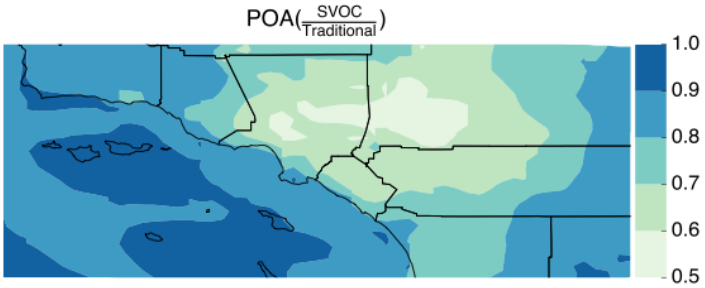

Figure S4: Ratio of the 14-day averaged POA mass concentration from the SVOC simulation to that from the Traditional simulation.

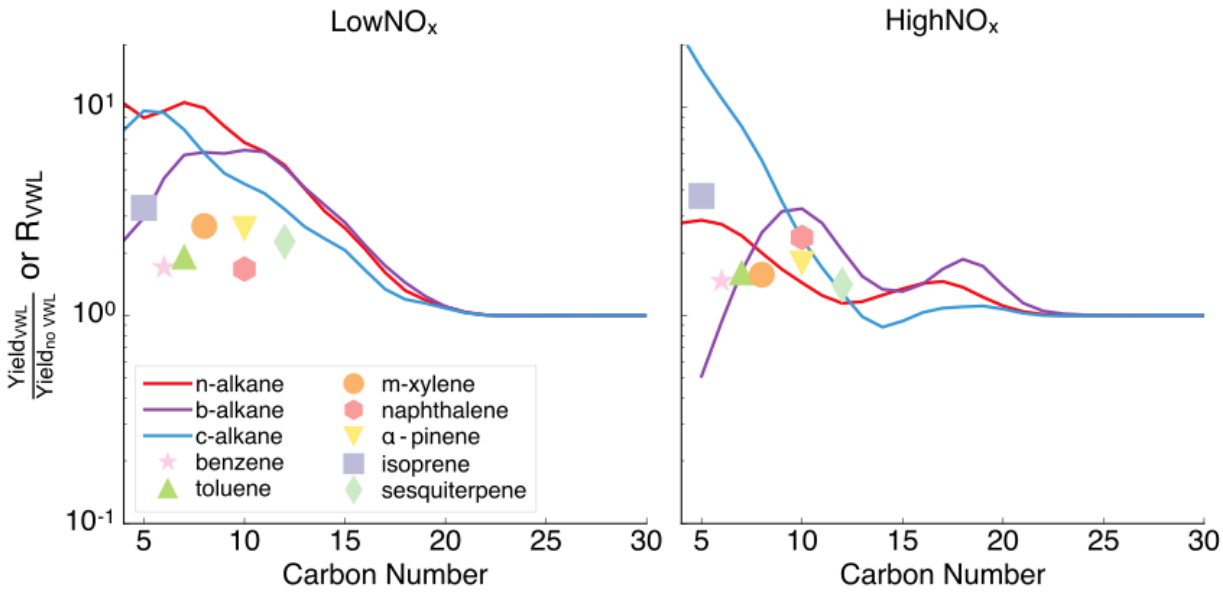

Figure S5: Vapor wall loss-related enhancements in SOA mass yield calculated using a box model version of the SOM for different precursor species at an organic aerosol mass concentration of 9 µg m^{-3}.

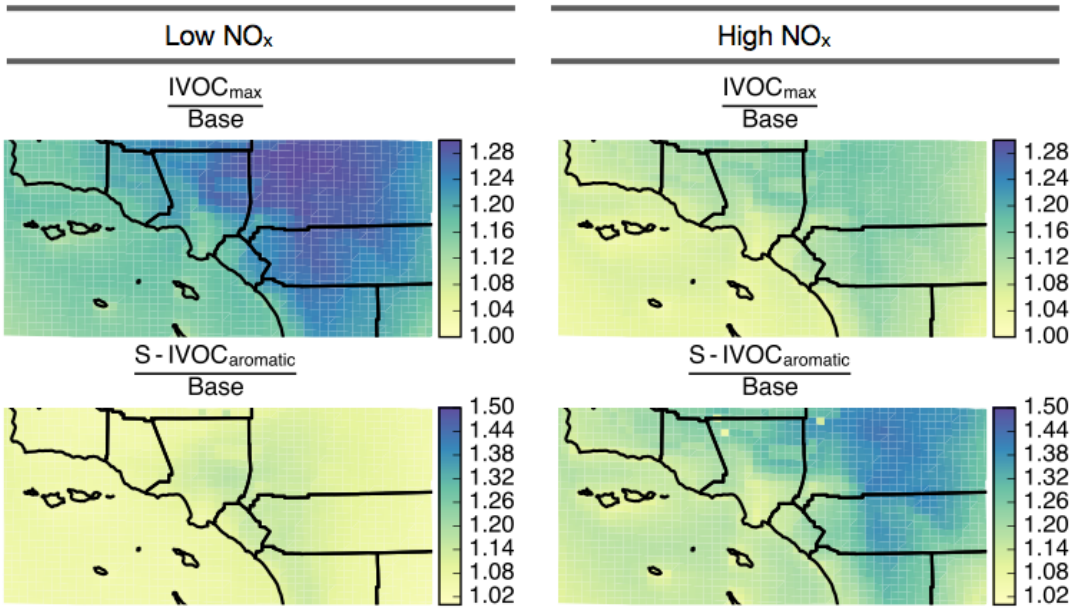

Figure S6: Ratio of the 14-day averaged OA mass concentration from the (a) $IVOC_{max}$ and (b) $IVOC_{aromatic}$ simulation to that from the Base simulation.

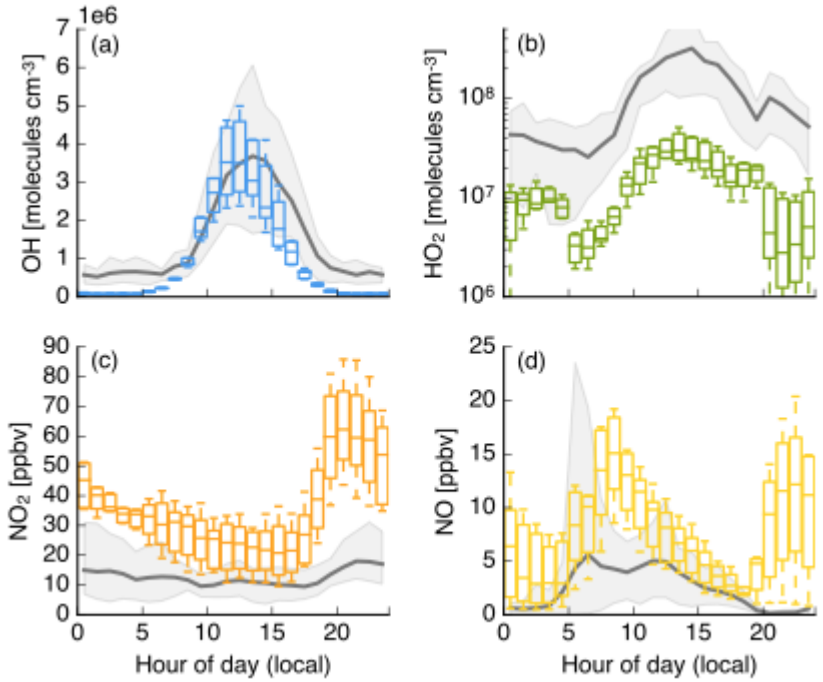

Figure S7: Modeled (2005) and measured (2010) diurnal profiles of (a) OH, (b) HO_2 (model), HO_2 (measurements) (c) NO_2 and (d) NO concentrations over Pasadena. Model predictions are shown as box plots while measurements are show as bands (10-90th percentiles) and a solid black line (median).*

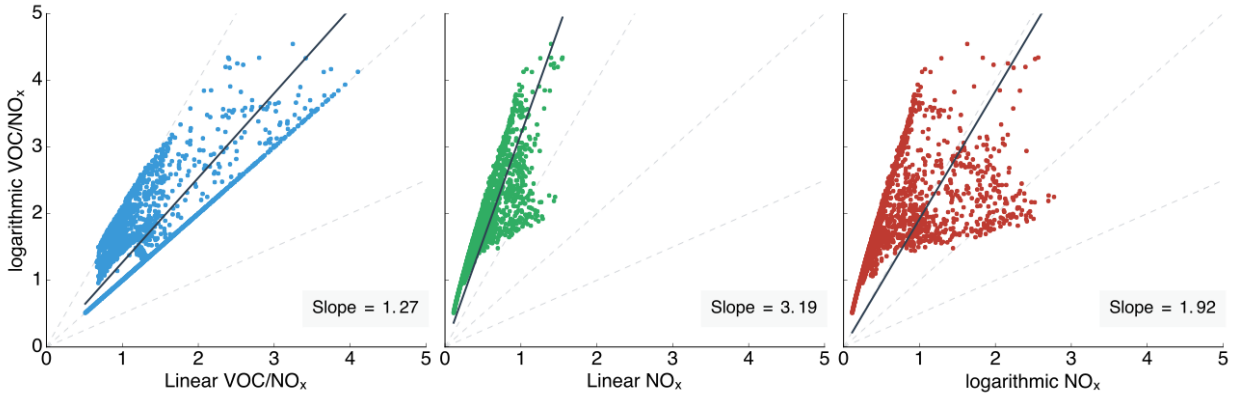

Figure S8: Scatter plots comparing model predictions of SOA_{eff} using equation 2 (logarithmic dependence on the VOC:NO_X ratio) to those predicted using (a) equation 1 (linear dependence on the VOC:NO_X ratio), (b) equation 3 (linear dependence on the NO_X concentration), and (c) equation 4 (logarithmic dependence on the NO_X concentration).

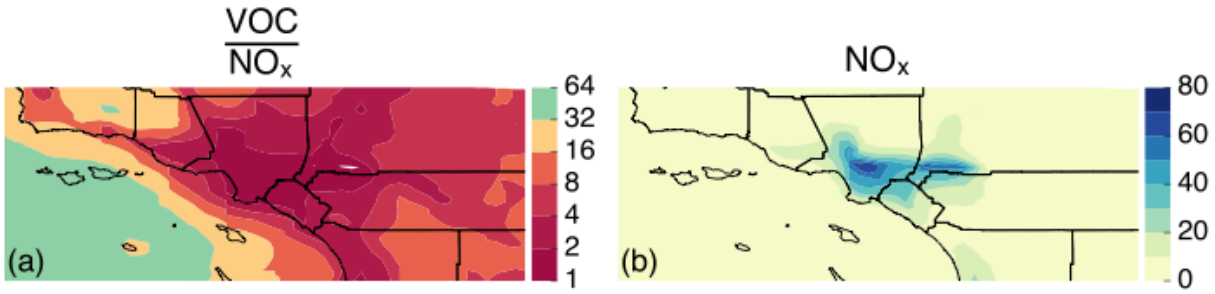

Figure S9: 14-day averaged (a) VOC:NO_X ratios (ppbv ppbv^{-1}) and (b) NO_X concentrations (ppbv) in southern California.

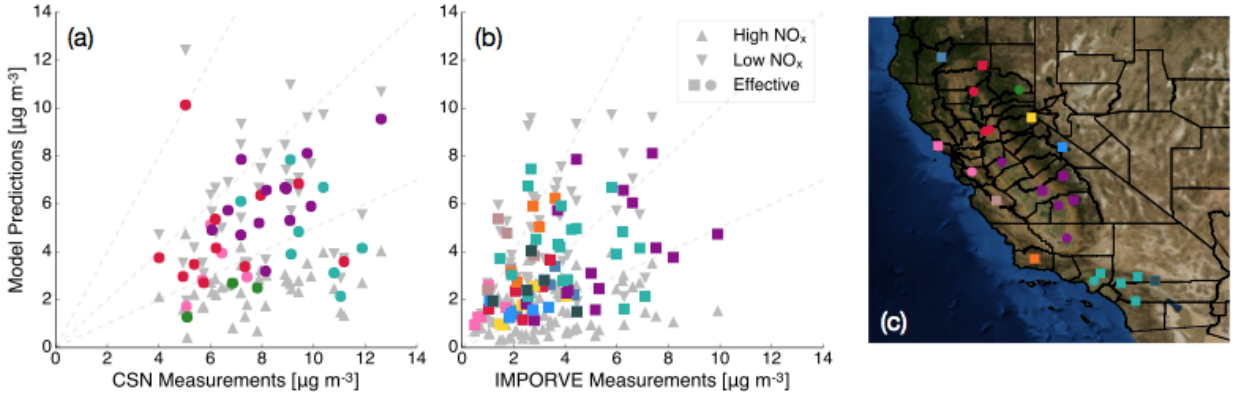

Figure S10: Model-measurement comparison for daily-averaged OA mass concentrations at (a) CSN and (b) IMPROVE sites across California. Panel (c) shows the color-coded geographic locations where the comparisons were made.

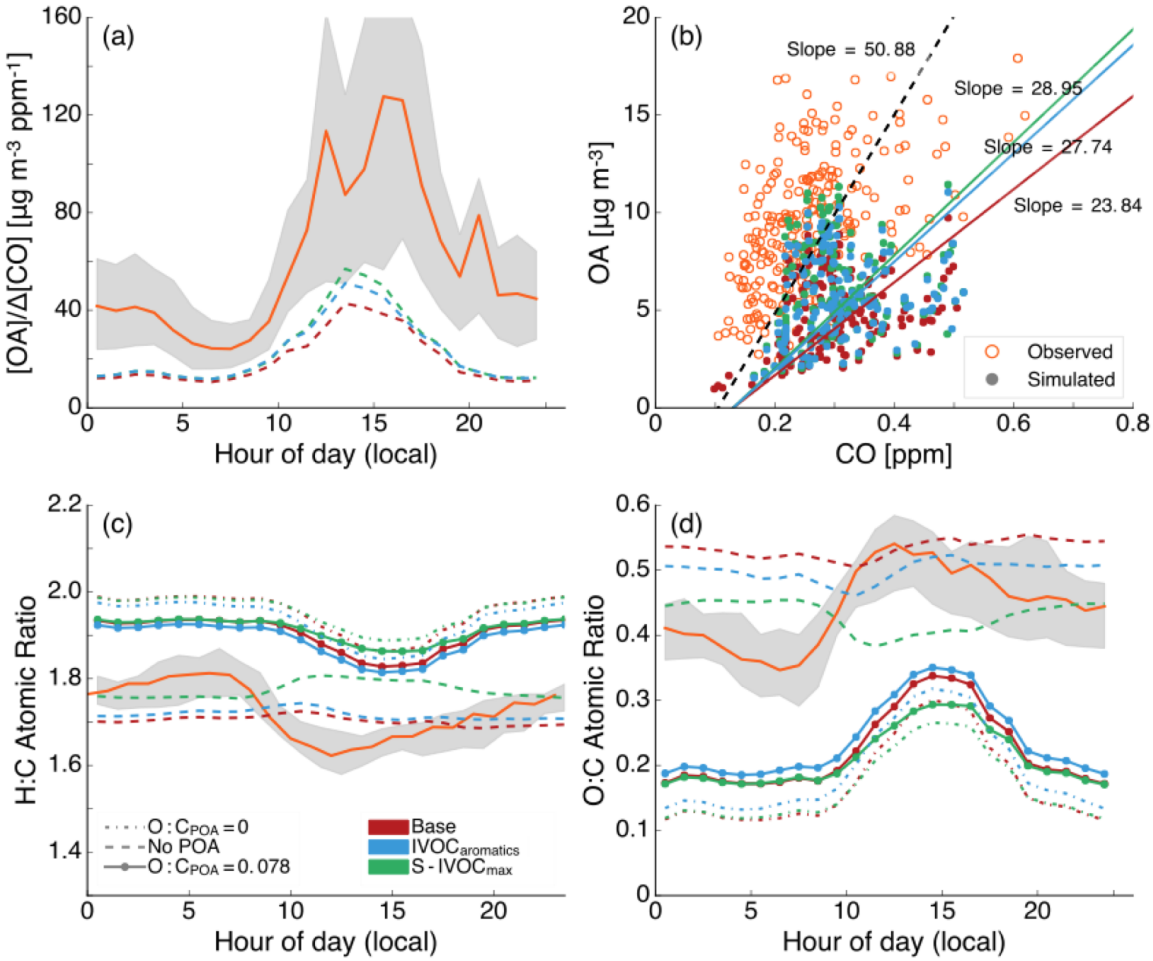

Figure S11: (a) Diurnal profile of the modeled and measured OA/ΔCO ratios at Riverside, CA. The box plots capture the 10^{th}-25^{th}-50^{th}-75^{th}-90^{th} in model predictions over the simulated episode while the gray bands and solid orange line represent the 10^{th} and 90^{th} percentile and median of the measured data. (b) Modeled and measured OA mass concentrations plotted against CO concentrations between 10 am and 8 pm local time. The solid and dashed black lines represent lines fitted to the modeled and measured data by forcing the X-intercept to be the corresponding modeled and measured background CO concentration. Diurnal profiles of the modeled and measured (c) H:C and (d) O:C ratios of the OA. The three different predictions show results from the Base simulations for OA assuming no change, the POA O:C was fixed to 0.078, and no POA. Model predictions are from three different simulations: Base, $IVOC_{max}$, and $S\text{-}IVOC_{aromatic}$.

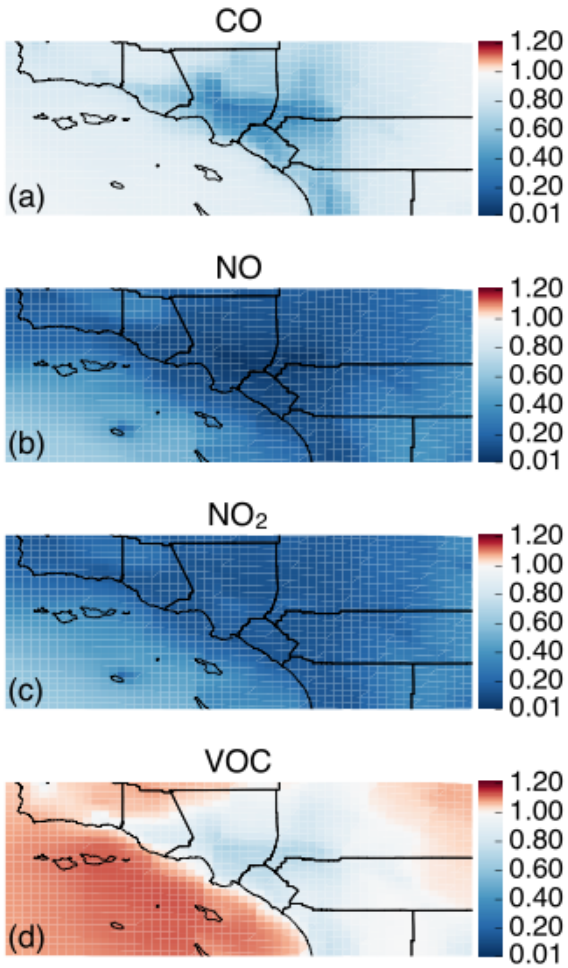

Figure S12: Ratios of 14-day averaged model predictions of (a) CO, (b) NO, (c) NO_2, and (d) VOC from 2035 to those from 2005. The 2035 simulations were performed with 2005 meteorological inputs but scaling the anthropogenic emissions for CO, NO_X, VOC, $PM_{2.5}$, SO_2, and NH_3 based on changes projected by the California Emission Projections and Analysis Model (CARB, 2018).

Tables

Table S1: Hydrocarbon distribution used to distribute POA emissions.

Carbon No.	C* (μg m^{-3})	ξ (fraction)		
		Gasoline	Diesel	Biomass Burning / Food Cooking
10	5.95e+06	0.0000	0.0031	0.0000
11	2.01e+06	0.0000	0.0001	0.0166
12	6.78e+05	0.0000	0.0000	0.0386
13	2.29e+05	0.0000	0.0001	0.0391
14	7.72e+04	0.0000	0.0000	0.0405
15	2.60e+04	0.1000	0.0000	0.0443
16	8.79e+03	0.0339	0.0001	0.0534
17	2.96e+03	0.0234	0.0583	0.0678
18	1.00e+03	0.0123	0.0427	0.0717
19	3.38e+02	0.0212	0.0548	0.0668
20	1.14e+02	0.0611	0.0943	0.0966
21	3.80e+01	0.1079	0.1462	0.0947
22	1.30e+01	0.1277	0.1809	0.0329
23	4.38e+00	0.1105	0.1775	0.0299
24	1.48e+00	0.0762	0.1368	0.0870
25	4.98e-01	0.0553	0.0775	0.0159
26	1.68e-01	0.0606	0.0262	0.0000
27	5.67e-02	0.0751	0.0004	0.0000
28	1.91e-02	0.0706	0.0003	0.0873
29	6.46e-03	0.0438	0.0001	0.1167
30	2.18e-03	0.0174	0.0001	0.0000